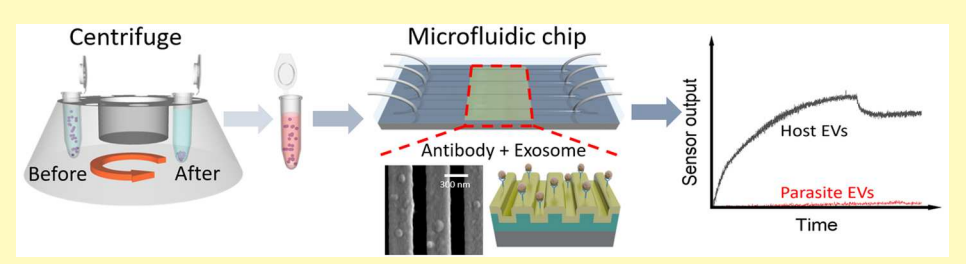


# Rapid Differentiation of Host and Parasitic Exosome Vesicles Using Microfluidic Photonic Crystal Biosensor

Yifei Wang,<sup>†</sup> Wang Yuan,<sup>‡</sup> Michael Kimber,\*,<sup>‡</sup> Meng Lu,\*,<sup>†</sup>,<sup>§</sup>,||<sub>©</sub> and Liang Dong\*,<sup>†</sup>,<sup>§</sup>

Supporting Information



ABSTRACT: Parasite extracellular vesicles (EVs) are potential biomarkers that could be exploited for the diagnosis of infectious disease. This paper reports a rapid bioassay to discriminate parasite and host EVs. The EV detection assay utilizes a label-free photonic crystal (PC) biosensor to detect the EVs using a host-specific transmembrane protein (CD63), which is present on EV secreted by host cells (modeled by murine macrophage cell line J774A.1) but is not expressed on EV secreted by parasitic nematodes such as the gastrointestinal nematode Ascaris suum. The surface of PC is functionalized to recognize CD63, and is sensitive to the changes in refractive index caused by the immobilization of EVs. The biosensor demonstrates a detection limit of 2.18 × 10<sup>9</sup> EVs/mL and a capability to characterize the affinity constants of antibody-host EV bindings. The discrimination of murine host EVs from parasite EVs indicates the capability of the sensor to differentiate EVs from different origins. The label-free, rapid EV assay could be used to detection parasite infection and facilitate the exosome-based clinic diagnosis and exosome research.

KEYWORDS: exosome, label-free assay, parasite infection, photonic crystal biosensor, immunosensor

R ecently, membranous extracellular vesicles (EVs), including nanoscale exosomes and other vesicles derived from cancer cells, have also been found in the blood of cancer patients. 1-3 These membrane-bound phospholipid nanovesicles are actively secreted by both prokaryotic and eukaryotic cells, including mammalian cells and pathogens like parasitic helminths.<sup>4–6</sup> EVs secreted from helminths contain effector molecules such as functional proteins and small RNAs, and as with other systems. There is emerging evidence demonstrating that EVs released from helminths could traffic within the host's body fluid and interact with the immune system to modulate the host immune response. -EVs have also been considered an important mediator of the cell to cell communication; because of the membrane-based structure, they are more stable than proteins and nucleotides biomarkers that are secreted alone, which arouses the potential to use EVs to diagnose infectious diseases and other human diseases like cancer.

Rapid, multiplexed exosome analysis can be used to detect minute amounts of various biomarkers for diseases that are currently difficult to diagnose and monitor such as cancer, infectious, autoimmune, and degenerative diseases. Fluorescence-based approaches, such as bead-based assays, have the multiplexing capability and high sensitivity but require excessive volumes of serum. 10,11 Compare to conventional methods based on immunoblotting or enzyme-linked immunosorbent assay (ELISA) assays,  $^{12-15}$  the PC-based label-free assay eliminates the labeling step. The outputs of PC-based devices can be measured in real time and the assay time can be significant reduced. 16-20 Recently, several biosensors have been reported for the analysis of exosomes, 21-27 using surface plasmonic resonance,<sup>22</sup> nuclear magnetic resonance,<sup>26</sup> and electrochemical aptasensor.<sup>27</sup>

The paper reports the discrimination of EVs derived from murine macrophages and parasites using a photonic crystal (PC) biosensor. The PC biosensor, consisting of a subwavelength grating, is essentially a narrowband optical reflector that reflects a particular wavelength of a broadband excitation. The capture of EVs on the biosensor increases the refractive index on the sensor surface and results in a change in the light reflectance of the PC. Using the PC biosensor, we have developed a label-free binding assay to detect EVs according to their membrane-specific proteins, and distinguish EVs secreted by a murine macrophage cell line (J774A.1) and a parasitic nematode (Ascaris suum). In addition, the developed

Received: May 3, 2018 Accepted: August 30, 2018 Published: August 30, 2018

<sup>&</sup>lt;sup>†</sup>Department of Electrical and Computer Engineering, <sup>‡</sup>Department of Biomedical Sciences, <sup>§</sup>Microelectronics Research Centre, and Department of Mechanical Engineering, Iowa State University, Ames, Iowa 50011, United States

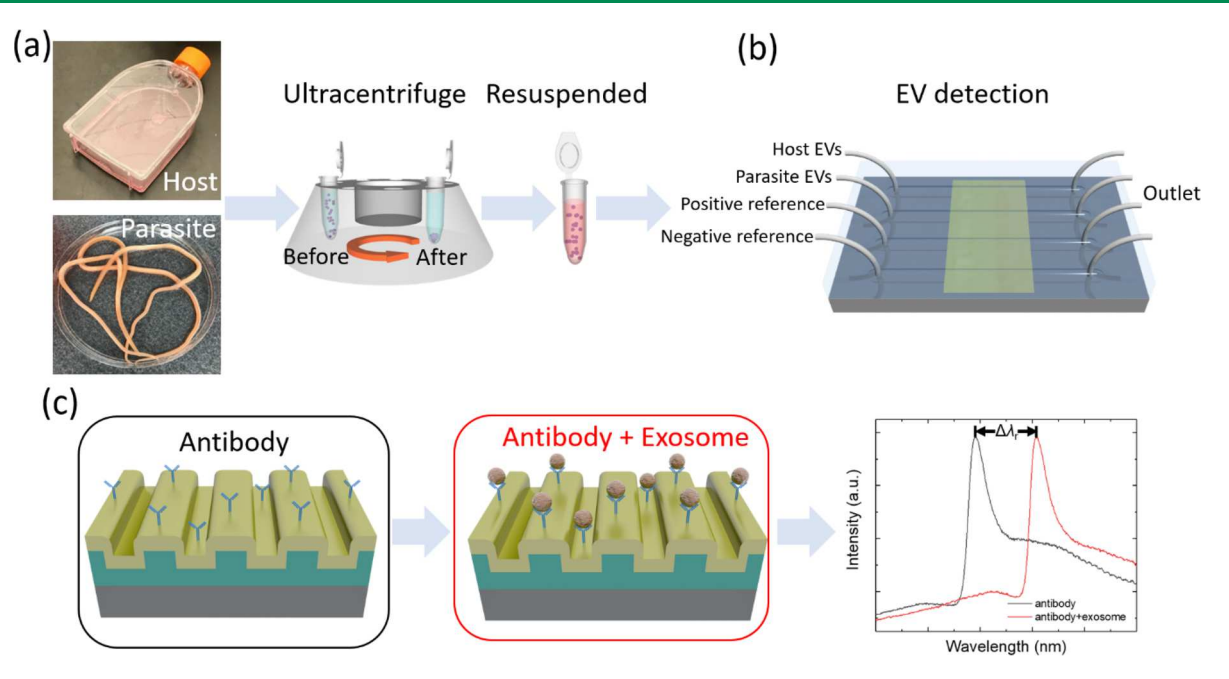


Figure 1. (a) Schematic diagram of the extraction of EVs from culture media. The EVs samples are centrifuged and resuspended before being flowed into the microfluidic chip. (b) Illustration of the microfluidic PC biosensor chip. Four channels are designed for the host, parasitic, positive, and negative reference samples, respectively. (c) Schematic structure of the PC grating and the label-free detection mechanism. The PC surface functionalized with the antibody (black box) exhibits resonant reflection (black curve in the reflection spectra). The binding of EVs to the antibody (red box) shift the narrowband reflection by a spectral shift of  $\Delta \lambda_r$ .

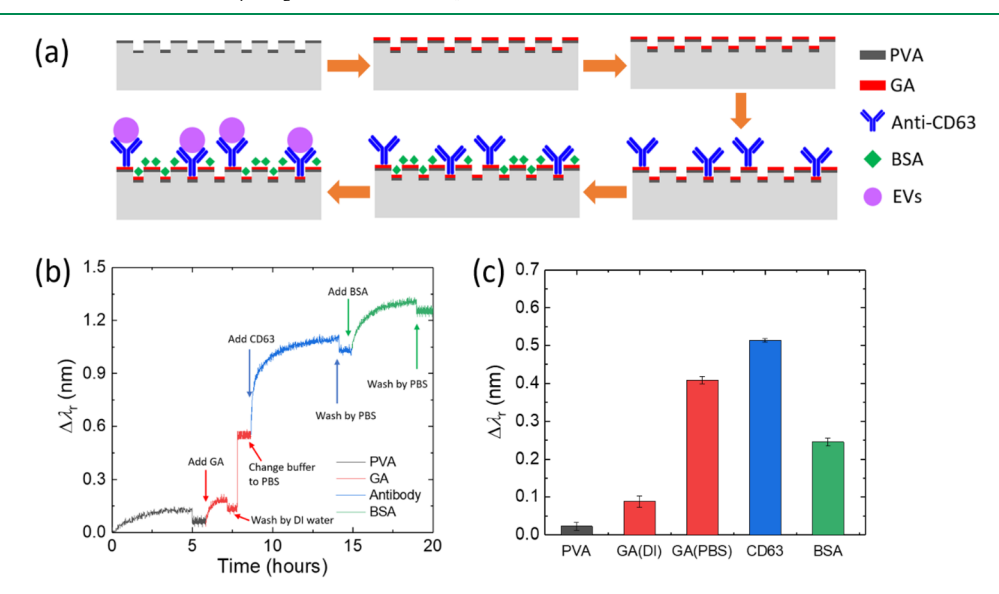


Figure 2. (a) Flowchart for the functionalization of the PC biosensor. (b) Measured wavelength shift as a function of time during the functionalization process. The black, red, blue, and green portions of the curve denote the PVA, GA, antibody, and BSA coating. (c) Resonant wavelength shift of the sensor after each step of the real-time measurement shown in (b).

assay can measure the binding of EV to its ligand in real time, thus enabling characterization of the EV-antibody binding affinity.

#### EXPERIMENTAL SECTION

Preparation of Host and Parasite EV Samples. The host and parasite EVs were isolated from spent murine macrophage and parasitic nematode culture media, respectively. Murine macrophage cell line (J774A.1) were cultured in DMEM containing 10% FBS (Thermo Fisher Scientific, Waltham, MA), 100 units of penicillin (Thermo Fisher Scientific, Waltham, MA), 100 μg/mL of streptomycin (Thermo Fisher Scientific, Waltham, MA), and 2 mM L-glutamine (Sigma-Aldrich, St. Louis, MO). Female adult *Ascaris* 

suum were collected from a local abattoir and maintained in Ascaris Ringer's solution at 37 °C. Culture media was collected after 24 h and filtered using 0.22  $\mu$ m syringe filters (Millipore Sigma, Burlington, MA) to remove debris then EV were purified by differential centrifugation as previously described. The EV pellets were resuspended in 100  $\mu$ L PBS solution and stored in a -80 °C freezer. The presence of EVs in these isolated preparations was confirmed using Nanoparticle Tracking Analysis (NanoSight LM10, Malvern Instruments, Malvern, UK). Figure 1a illustrates the process of preparing membranous extracellular vesicles, including nanoscale exosomes. The details of the materials and supplies are given in the Supporting Information.

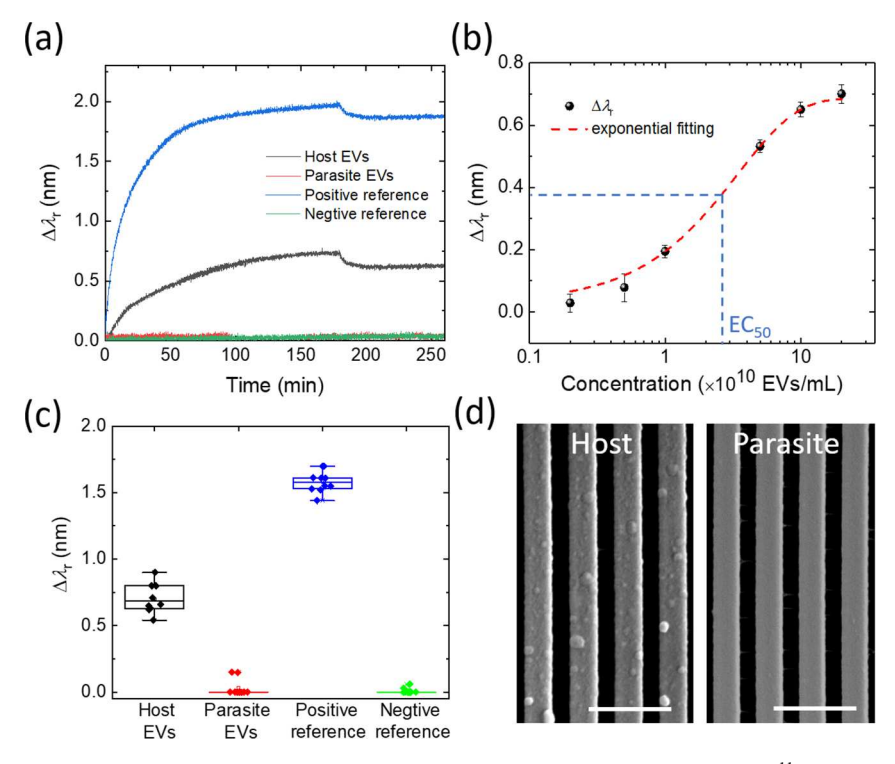


Figure 3. (a) Kinetic binding of anti-CD63 with host and parasite EVs at the concentration of  $c=2\times10^{11}$  EVs/mL. (b) Measured resonance wavelength shifts as a function of 6 different concentrations of EVs from  $2\times10^9$  EVs/mL to  $2\times10^{11}$  EVs/mL. The experiment data is fitted (red dash curve) and the EC<sub>50</sub> is determined by the blue dash lines. (c) Box plot of the  $\Delta\lambda_r$  for host and parasite EVs at  $2\times10^{11}$  EVs/mL in comparison to the results of positive and negative references. (d) SEM images of the host and parasite EVs immobilized on the PC surface at the concentrations of  $2\times10^{11}$  EVs/mL. Scale bar: 1  $\mu$ m.

PC Biosensors Embedded in Microfluidic Channels. The PC biosensor used in this study consists of a one-dimensional (1D) grating substrate, which is coated with a high-refractive-index thin film as shown in Figure 1b. The high-refractive-index thin film acts as a light confinement layer and supports the resonance modes that are evanescently confined to the PC surface. The grating modulation allows the phase matching of excitation light to the PC resonances and results in the narrowband reflection.<sup>28</sup>

The PC biosensors can detect chemicals and biomolecules via the biochemical interactions occurring on their surfaces. The adsorbed molecules on the sensor surface cause a change in the effective refractive index, which shifts the peak in the reflectance. The amount of spectral shift is proportional to the concentration of the target molecule as shown in Figure 1c. Since its early demonstration, <sup>29</sup> the PC biosensor has gained significant attentions and been utilized for the analysis of various biomaterials, such as pathogens, DNA, proteins, enzymes, cells, and toxins. <sup>29–32</sup>

The details of the PC fabrication and readout instrument are described in the Supporting Information. In brief, the submicron grating structure of the PC biosensor was fabricated inexpensively using the nanoreplica molding method.<sup>33</sup> The molding silicon stamp (LightSmyth Technologies, Eugene, OR) carries a 1D grating with a period of 555.5 nm. The grating pattern was replicated on the surface of glass coverslip using UV curable epoxy (Norland Products, Cranbury, NJ). A titanium oxide (TiO2) was deposited on the replicated grating. To facilitate the detection of EVs, the fabricated PC structures were incorporated with microfluidic channels as shown in Figure 1b. Four microfluidics channels were created, and each channel contained the PC grating (0.5 mm × 4 mm) in the middle. A broadband white light (Ocean Optics, Largo, FL) was used as the excitation and the light reflected off the PC grating was analyzed using a compact spectrometer (Ocean Optics, Largo, FL).<sup>34</sup> The measured reflection spectra were analyzed to find the peak reflection wavelength  $(\lambda_r)$ . The optical readout system was positioned below the microfluidic chip and aligned to the PC regions one at a time.

Before the sensors are used for the EV analysis, we functionalized the sensor surface using the EV specific antibody. The PC biosensor with the antibody coating is illustrated in the Figure 1b. When the EVs bind to the antibodies (red box in Figure 1b), the reflection peak wavelength will redshift (Figure 1c) and the amount of wavelength shift  $(\Delta \lambda_{\rm r})$  will correspond to the concentration of EVs.

### ■ RESULTS AND DISCUSSION

Surface Functionalization for the PC Biosensor. Before the PC biosensor was used for the analysis of EVs, we functionalized the sensor surface using a four-step process.<sup>35</sup> Figure 2a summarizes the major steps of the functionalization process (see details in the Supporting Information). During the process, the resonant wavelength shift was recorded every 2 s and plotted in Figure 2b. The initial step (black line in Figure 2b) was the coating of a porous polymer layer (Polyvinylamine, PVA) that can provide a high-density amine group. The PVA coating process lasted 5 h and was followed by a wash using DI water. Then, a bifunctional linker, glutaraldehyde (GA), was pumped into the channels. After 1.5 h incubation (red line in Figure 2b), the channels were washed using DI water. Before the solution of capture antibody, anti-CD63, was introduced into the channels, the buffer solution was changed to the PBS (pH = 7.4) and the resonance wavelength was measured. The anti-CD63 solution (0.1 mg/mL) was incubated inside the channels for overnight and then washed using the PBS solution. The final step was using the bovine serum albumin (BSA) solution (0.5% in 0.85% sodium chloride) to block the unoccupied aldehyde groups on the GA layer for 4 h. The results of the anti-CD63 coating and BSA blocking are shown in Figure 2b as the blue and green portions, respectively. After the BSA blocking, the biosensors

were ready for the analysis of EVs. The 4-step functionalization process took less than 20 h, which can be optimized in the future.

Figure 2c summarizes the resonant wavelength shift after each step of the process based on the real-time measurement shown in Figure 2b. The first two columns in Figure 2c represent the sensor signals after PVA and GA coatings. The wavelength shifts are approximately  $\Delta\lambda_{\rm r}=0.15$  and 0.2 nm, respectively. The third column shows ~0.4 nm wavelength shift owing to the change of buffer from DI water to PBS. The absorption of the anti-CD63 and BSA blocker results in  $\Delta\lambda_{\rm r}$  ~0.5 nm and ~0.25 nm, respectively. The measured resonance wavelength shift for each step was calculated based on the previous step. In each column, the error bar was the standard deviation calculated using nine independent measurements from nine PC sensors.

## Detection of EVs Secreted by Murine Macrophages.

As a label-free detection approach, the PC biosensor can monitor the analyte-ligand binding process by recording the sensor output in real time. The host EVs were extracted from the murine macrophage cell culture and prepared to obtain a concentration of  $2 \times 10^{11}$  EVs/mL. Figure 3a shows the sensor output over time when the host and parasite EV solution was flowed through the microfluidic channel at a flow rate 30  $\mu$ L/ min. The reflection spectrum was measured every 2 s and the  $\Delta \lambda_r$  values were calculated. After 180 min, the ligand-analyte binding reached an equilibrium. Then, we washed the channels using PBS to remove the unbounded EVs and let the binding process enter the dissociate phase. After the PBS wash, the EVs binding results in a  $\Delta \lambda_r$  of approximately 0.7 nm. The positive and negative reference experiments were tested using the biosensor. For the positive reference experiment, the GAcoated PC biosensors were used to capture EVs without targeting a specific membrane protein. The positive reference experiment exhibited an output of  $\Delta \lambda_r = 1.8$  nm. In contrast, the negative reference experiments were carried out on the BSA-blocked PC surface without anti-CD63 antibody. The sensor output is nearly zero for the negative reference experiment. The details of the reference experimental processes are given in Supporting Information. As shown in the sensorgrams in Figure 3a, the label-free signals still slowly increase at the saturation region. According to the pervious study<sup>36</sup> on the label-free sensorgrams, our dynamic response curves in Figure 3a include both the binding reaction and the EV diffusion processes. To identify the limit of detection (LOD), we measured host EV samples at a dilution serial of six concentrations ranging from  $2 \times 10^9$  EVs/mL to  $2 \times 10^{11}$ EVs/mL. The samples were diluted consecutively by a factor of 2 in PBS. Figure 3b shows the dose-response curve,  $\Delta \lambda_r$ versus EV concentration, in logarithmic scale. At  $2 \times 10^{11}$  EVs/ mL, the sensor output starts to saturate with  $\Delta \lambda_r = 0.7$  nm. The dose-response data was fitted with a sigmoidal curve (the red line in Figure 3b) with a reduced chi-squared ( $\chi^2$ ) value of 0.854. The error bar in the dose—response curve represents the standard deviation ( $\sigma$ ) of  $\Delta \lambda_r$  measured using nine different PC biosensors. The LOD of this sensor was calculated by the summation of the noise signal arising from the negative reference and the  $3\sigma$  of the EV sample at the lowest concentration. The LOD is found to be  $2.18 \times 10^9$  EVs/mL that falls in the range of the clinically relevant concentration of EVs from  $1 \times 10^8$  to  $3 \times 10^{12}$  exosomes/mL.  $^{37-39}$  Therefore, the presented sensor will find it useful in applications of clinic diagnosis. The value of the equilibrium dissociation constant,

 $K_{\rm D}$ , can be determined by the ligand half maximal effective concentration (EC<sub>50</sub>) based on the Michaelis–Menten equation. <sup>40,41</sup> In our case, based on the obtained dose response in Figure 3b, the value of  $K_{\rm D}$  was found to be EC<sub>50</sub> = 2.36 ×  $10^{10}$  EVs/mL using the fitted curve (see red dashed curve).

Differentiation of Host and Parasite EVs. In the present study, the surface protein chosen to distinguish the EVs that are released by the host and the helminth is CD63, which is a well-established exosome marker. Recent studies showed that CD63 presents on the surface of other vesicles too. However, ongoing proteomic analysis by our group demonstrates that the EVs released from Ascaris suum do not contain the homologue of CD63, and that CD63 homologues are not found in the Ascaris genome. The absence of these proteins strongly suggests that the composition of Ascaris suum EVs is different to that from the host cells. Indeed, recent analysis by our group suggests parasite-derived EVs have widespread species- and stage-specific protein composition. Such differences in surface protein expression allows us to develop the EV differentiation assay.

The box plot in Figure 3c shows the resonance wavelength shift for host and parasite exosome detection with the positive reference and negative reference. Bars indicate mean and 25th and 75th percentiles and lines indicate mean  $\pm 1.5$  times the interquartile range. From the box plot in Figure 3c, the exosome vesicles from the host with a concentration of 2  $\times$ 10<sup>11</sup> EVs/mL have around 0.7 nm resonance wavelength shift, with this value between the positive reference and negative reference experiment. The detection of the parasite EVs using the anti-CD63 antibody-coated PC sensor generated a nearly zero output. For the positive reference experiment, the EVs were captured regardless of the type of transmembrane proteins. The positive reference experiment shows a signal of 1.6 nm shift. Figure 3c demonstrates the capability to discriminate EVs from host cells and parasites. Compared to the host EVs, the parasite EVs do not carry CD63 antigens. The details of the PC sensor outputs of the parasite EVs, its positive reference, and negative reference experiments are shown in the Supporting Information. The reference experiment can be used to estimate the noise level of our sensor system. As shown in Figure 3c, the overall system noise level is 0.03 nm, which can be calculated using the standard deviation of the negative reference test. The label-free assay can be utilized to diagnose infectious disease using EVs. Figure 3d shows the scanning electron microscope (SEM) image of the host EVs and parasite EVs immobilized on the PC surface at the concentrations of  $2 \times 10^{11}$  EVs/mL. The average size of the EVs is approximately 100 nm. The PC-based label-free assay can be used for the rapid differentiation of exosome vesicles from host and parasite in 2 h.

#### CONCLUSIONS

In summary, we have demonstrated the use of the PC biosensor for rapid and specific discrimination of EVs extracted from the culture media; furthermore, incorporation of the PC biosensor into microfluidic channels allows for parallel quantification of EVs from different sources. The advantages of the PC-based label-free assay include the low-cost and disposable sensor, short assay time, and improved spectral sensitivity. The PC biosensors are less expensive than the gold coated nanohole array used in work of H. Im et al. <sup>22</sup> Compared with the SPR device, the narrower line width of the PC resonance enables the detection of EVs without using a

signal enhancer. Simplicity of the PC-based EV assay would permit detection in nonlaboratory settings, thus eliminating the use of additional label reagents. The obtained LOD for precleaned EV samples is  $2.18 \times 10^9$  EVs/mL. We expect that the detection limit may be further improved through the use of nanoparticles to enhance the sensor signal or by optimizing the PC structure to achieve resonances with reduced spectral line width. 44,45 This work focused on a single exosomal protein marker but EVs membrane carries more than one markers. The analysis of multiple exosomal markers simultaneously will allow tracking the origin of EVs in complex samples such as blood. Our future work will utilize the PC-based microarray technology<sup>46</sup> to generate a profile of surface protein markers on the target EVs. With minimal sample processing, simple assay, and high throughput, the implementation of PC biosensor will enable EV analysis in point-of-care applications, such as diagnosis of parasite infections in the near future.

#### ASSOCIATED CONTENT

## S Supporting Information

The Supporting Information is available free of charge on the ACS Publications website at DOI: 10.1021/acssensors.8b00360.

Materials and supplies, process for the fabrication of the PC sensor, the label-free EV assay protocol, the positive and negative reference experiments, kinetic binding curve, ROC curve, and ELISA analysis results (PDF)

#### AUTHOR INFORMATION

## **Corresponding Authors**

\*E-mail: michaelk@iastate.edu. \*E-mail: menglu@iastate.edu. \*E-mail: ldong@iastate.edu.

ORCID

Meng Lu: 0000-0001-7444-6759

Notes

The authors declare no competing financial interest.

## ■ ACKNOWLEDGMENTS

This work was supported by the United States National Science Foundation under Grant Nos. ECCS 17-11839 and ECCS 16-53673. Any opinions, findings, and conclusions or recommendations expressed in this material are those of the authors and do not necessarily reflect the views of National Science Foundation. This work was supported by an HIH R21 award (AI117204) to MJK. The authors thank the Nano Fabrication Centre at the University of Minnesota for the support of device fabrication. YW acknowledges the Catron Center for Solar Energy Research for the Carton Graduate Fellowship.

## **■** REFERENCES

- (1) Bard, M. P.; Hegmans, J. P.; Hemmes, A.; Luider, T. M.; Willemsen, R.; Severijnen, L. A. A.; van Meerbeeck, J. P.; Burgers, S. A.; Hoogsteden, H. C.; Lambrecht, B. N. Proteomic analysis of exosomes isolated from human malignant pleural effusions. *Am. J. Respir. Cell Mol. Biol.* **2004**, *31* (1), 114–121.
- (2) Pant, S.; Hilton, H.; Burczynski, M. E. The multifaceted exosome: Biogenesis, role in normal and aberrant cellular function, and frontiers for pharmacological and biomarker opportunities. *Biochem. Pharmacol.* **2012**, *83* (11), 1484–1494.

(3) Simpson, R. J.; Lim, J. W. E.; Moritz, R. L.; Mathivanan, S. Exosomes: proteomic insights and diagnostic potential. *Expert Rev. Proteomics* **2009**, *6* (3), 267–283.

- (4) Buck, A. H.; Coakley, G.; Simbari, F.; McSorley, H. J.; Quintana, J. F.; Le Bihan, T.; Kumar, S.; Abreu-Goodger, C.; Lear, M.; Harcus, Y.; Ceroni, A.; Babayan, S. A.; Blaxter, M.; Ivens, A.; Maizels, R. M. Exosomes secreted by nematode parasites transfer small RNAs to mammalian cells and modulate innate immunity. *Nat. Commun.* **2014**, *5*, 5488.
- (5) Zamanian, M.; Fraser, L. M.; Agbedanu, P. N.; Harischandra, H.; Moorhead, A. R.; Day, T. A.; Bartholomay, L. C.; Kimber, M. J. Release of Small RNA-containing Exosome-like Vesicles from the Human Filarial Parasite Brugia malayi. *PLoS Neglected Trop. Dis.* **2015**, *9* (9), e0004069.
- (6) Thery, C.; Ostrowski, M.; Segura, E. Membrane vesicles as conveyors of immune responses. *Nat. Rev. Immunol.* **2009**, *9* (8), 581–593
- (7) Anthony, R. M.; Rutitzky, L. I.; Urban, J. F.; Stadecker, M. J.; Gause, W. C. Protective immune mechanisms in helminth infection. *Nat. Rev. Immunol.* **2007**, *7* (12), 975–987.
- (8) Hewitson, J. P.; Grainger, J. R.; Maizels, R. M. Helminth immunoregulation: The role of parasite secreted proteins in modulating host immunity. *Mol. Biochem. Parasitol.* **2009**, *167* (1), 1–11.
- (9) Maizels, R. M.; McSorley, H. J. Regulation of the host immune system by helminth parasites. *J. Allergy Clin. Immunol.* **2016**, *138* (3), 666–675.
- (10) Nolan, J. P.; Mandy, F. Multiplexed and microparticle-based analyses: Quantitative tools for the large-scale analysis of biological systems. *Cytometry, Part A* **2006**, *69a* (5), 318–325.
- (11) Banigan, M. G.; Kao, P.; Kozubek, J. A.; Winslow, A. R.; Medina, J.; Costa, J.; Schmitt, A.; Schneider, A.; Cabral, H.; Cagsal-Getkin, O.; Vanderburg, C. R.; Delalle, I. Differential Expression of Exosomal microRNAs in Prefrontal Cortices of Schizophrenia and Bipolar Disorder Patients. *PLoS One* **2013**, *8* (1), e48814.
- (12) Lequin, R. M. Enzyme Immunoassay (EIA)/Enzyme-Linked Immunosorbent Assay (ELISA). *Clin. Chem.* **2005**, *51* (12), 2415–2418.
- (13) Taylor, D. D.; Gercel-Taylor, C. Tumour-derived exosomes and their role in cancer-associated T-cell signalling defects. *Br. J. Cancer* **2005**, 92 (2), 305–311.
- (14) Alvarez, M. L.; Khosroheidari, M.; Ravi, R. K.; DiStefano, J. K. Comparison of protein, microRNA, and mRNA yields using different methods of urinary exosome isolation for the discovery of kidney disease biomarkers. *Kidney Int.* **2012**, 82 (9), 1024–1032.
- (15) Jorgensen, M. M.; Baek, R.; Varming, K. Potentials and capabilities of the Extracellular Vesicle (EV) Array. *J. Extracell. Vesicles* **2015**, *4*, 26048.
- (16) Lu, M.; Choi, S.; Wagner, C. J.; Eden, J. G.; Cunningham, B. T. Label free biosensor incorporating a replica-molded, vertically emitting distributed feedback laser. *Appl. Phys. Lett.* **2008**, 92 (26), 261502.
- (17) Chen, W.; Long, K.; Lu, M.; Chaudhery, V.; Yu, H.; Choi, J. S.; Polans, J.; Zhuo, Y.; Harley, B. A. C.; Cunningham, B. T. Photonic crystal enhanced microscopy for imaging of live cell adhesion. *Analyst* **2013**, *138* (20), 5886–5894.
- (18) Liu, L.; Xu, Z.; Dong, L.; Lu, M. Angular spectrum detection instrument for label-free photonic crystal sensors. *Opt. Lett.* **2014**, 39 (9), 2751–2754.
- (19) Sun, T.; Kan, S.; Marriot, G.; Chang-Hasnain, C. High-Contrast Grating Resonator for Label-Free Biosensors. 2015 Conference on Lasers and Electro-Optics (CLEO), 2015; pp STu4K-6.
- (20) Wang, Y.; Ali, A.; Chow, E.; Dong, L.; Lu, M. An optofluidic metasurface for lateral flow-through detection of breast cancer biomarker. *Biosens. Bioelectron.* **2018**, *107*, 224–229.
- (21) Goda, T.; Masuno, K.; Nishida, J.; Kosaka, N.; Ochiya, T.; Matsumoto, A.; Miyahara, Y. A label-free electrical detection of exosomal microRNAs using microelectrode array. *Chem. Commun.* **2012**, *48* (98), 11942–11944.

(22) Im, H.; Shao, H.; Park, Y. I.; Peterson, V. M.; Castro, C. M.; Weissleder, R.; Lee, H. Label-free detection and molecular profiling of exosomes with a nano-plasmonic sensor. *Nat. Biotechnol.* **2014**, 32 (5), 490–U219.

- (23) Zhu, L.; Wang, K.; Cui, J.; Liu, H.; Bu, X.; Ma, H. L.; Wang, W.; Gong, H.; Lausted, C.; Hood, L.; Yang, G.; Hu, Z. Label-Free Quantitative Detection of Tumor-Derived Exosomes through Surface Plasmon Resonance Imaging. *Anal. Chem.* **2014**, *86* (17), 8857–8864.
- (24) Zubiri, I.; Posada-Ayala, M.; Sanz-Maroto, A.; Calvo, E.; Martin-Lorenzo, M.; Gonzalez-Calero, L.; de la Cuesta, F.; Lopez, J. A.; Fernandez-Fernandez, B.; Ortiz, A.; Vivanco, F.; Alvarez-Llamas, G. Diabetic nephropathy induces changes in the proteome of human urinary exosomes as revealed by label-free comparative analysis. *J. Proteomics* **2014**, *96*, 92–102.
- (25) Su, J. Label-Free Single Exosome Detection Using Frequency-Locked Microtoroid Optical Resonators. *ACS Photonics* **2015**, 2 (9), 1241–1245.
- (26) Lee, K.; Shao, H.; Weissleder, R.; Lee, H. Acoustic Purification of Extracellular Microvesicles. ACS Nano 2015, 9 (3), 2321–2327.
- (27) Wang, S.; Zhang, L.; Wan, S.; Cansiz, S.; Cui, C.; Liu, Y.; Cai, R.; Hong, C.; Teng, I. T.; Shi, M.; Wu, Y.; Dong, Y.; Tan, W. Aptasensor with Expanded Nucleotide Using DNA Nanotetrahedra for Electrochemical Detection of Cancerous Exosomes. *ACS Nano* **2017**, *11* (4), 3943–3949.
- (28) Fan, S.; Joannopoulos, J. D. Analysis of guided resonances in photonic crystal slabs. *Phys. Rev. B: Condens. Matter Mater. Phys.* **2002**, 65 (23), 1 DOI: 10.1103/PhysRevB.65.235112.
- (29) Inan, H.; Poyraz, M.; Inci, F.; Lifson, M. A.; Baday, M.; Cunningham, B. T.; Demirci, U. Photonic crystals: emerging biosensors and their promise for point-of-care applications. *Chem. Soc. Rev.* **2017**, *46* (2), 366–388.
- (30) Meade, S. O.; Chen, M.; Sailor, M. J.; Miskelly, G. M. Multiplexed DNA Detection Using Spectrally Encoded Porous SiO2 Photonic Crystal Particles. *Anal. Chem.* **2009**, *81* (7), 2618–2625.
- (31) Sharma, A. C.; Jana, T.; Kesavamoorthy, R.; Shi, L.; Virji, M. A.; Finegold, D. N.; Asher, S. A. A general photonic crystal sensing motif: Creatinine in bodily fluids. *J. Am. Chem. Soc.* **2004**, *126* (9), 2971–2977
- (32) Han, J.; Kim, H. J.; Sudheendra, L.; Gee, S. J.; Hammock, B. D.; Kennedy, I. M. Photonic Crystal Lab-On-a-Chip for Detecting Staphylococcal Enterotoxin B at Low Attomolar Concentration. *Anal. Chem.* **2013**, *85* (6), 3104–3109.
- (33) Block, I. D.; Chan, L.; Cunningham, B. T. Large-area submicron replica molding of porous low-k dielectric films and application to photonic crystal biosensor fabrication. *Microelectron. Eng.* **2007**, *84* (4), 603–608.
- (34) Wang, Y.; Huang, Y.; Sun, J.; Pandey, S.; Lu, M. Guided-mode-resonance-enhanced measurement of thin-film absorption. *Opt. Express* **2015**, 23 (22), 28567–28573.
- (35) Gallegos, D.; Long, K.; Yu, H.; Clark, P. P.; Lin, Y.; George, S.; Nath, P.; Cunningham, B. T. Label-free biodetection using a smartphone. *Lab Chip* **2013**, *13* (11), 2124–2132.
- (36) Glaser, R. W. Antigen-Antibody Binding and Mass-Transport by Convection and Diffusion to a Surface a 2-Dimensional Computer-Model of Binding and Dissociation Kinetics. *Anal. Biochem.* 1993, 213 (1), 152–161.
- (37) Ibn Sina, A. A.; Vaidyanathan, R.; Dey, S.; Carrascosa, L. G.; Shiddiky, M. J. A.; Trau, M. Real time and label free profiling of clinically relevant exosomes. *Sci. Rep.* **2016**, *6*, 30460.
- (38) de Vrij, J.; Maas, S. L. N.; van Nispen, M.; Sena-Esteves, M.; Limpens, R. W. A.; Koster, A. J.; Leenstra, S.; Lamfers, M. L.; Broekman, M. L. D. Quantification of nanosized extracellular membrane vesicles with scanning ion occlusion sensing. *Nanomedicine* **2013**, *8* (9), 1443–1458.
- (39) Huang, X. Y.; Yuan, T. Z.; Tschannen, M.; Sun, Z. F.; Jacob, H.; Du, M. J.; Liang, M. H.; Dittmar, R. L.; Liu, Y.; Liang, M. Y.; Kohli, M.; Thibodeau, S. N.; Boardman, L.; Wang, L. Characterization of human plasma-derived exosomal RNAs by deep sequencing. *BMC Genomics* **2013**, *14* (1), 319.

(40) Hulme, E. C.; Trevethick, M. A. Ligand binding assays at equilibrium: validation and interpretation. *Br. J. Pharmacol.* **2010**, *161* (6), 1219–1237.

- (41) Deichmann, U.; Schuster, S.; Mazat, J. P.; Cornish-Bowden, A. Commemorating the 1913 Michaelis-Mentenpaper Die Kinetik der Invertinwirkung: three perspectives. *FEBS J.* **2014**, *281* (2), 435–463.
- (42) Kowal, J.; Arras, G.; Colombo, M.; Jouve, M.; Morath, J. P.; Primdal-Bengtson, B.; Dingli, F.; Loew, D.; Tkach, M.; Thery, C. Proteomic comparison defines novel markers to characterize heterogeneous populations of extracellular vesicle subtypes. *Proc. Natl. Acad. Sci. U. S. A.* **2016**, *113* (8), E968–E977.
- (43) Harischandra, H.; Yuan, W.; Loghry, H.; Zamanian, M.; Kimber, M. Profiling extracellular vesicle release by the filarial nematode Brugia malayi reveals sex-specific differences in cargo and a sensitivity to ivermectin. *PLoS Neglected Trop. Dis.* **2018**, *12* (4), e0006438—e0006438.
- (44) Zhao, Y.; Cao, M.; McClelland, J. F.; Shao, Z.; Lu, M. A photoacoustic immunoassay for biomarker detection. *Biosens. Bioelectron.* **2016**, 85, 261–266.
- (45) Wang, Y.; Song, J.; Dong, L.; Lu, M. Optical bound states in slotted high-contrast gratings. *J. Opt. Soc. Am. B* **2016**, 33 (12), 2472–2479.
- (46) Huang, C.; George, S.; Lu, M.; Chaudhery, V.; Tan, R.; Zangar, R. C.; Cunningham, B. T. Application of Photonic Crystal Enhanced Fluorescence to Cancer Biomarker Microarrays. *Anal. Chem.* **2011**, 83 (4), 1425–1430.